

Surface Boundary Conditions Strongly Affect the Dynamics of Rotating Horizontal Convection

Z. Y. Ng and G. J. Sheard

Department of Mechanical and Aerospace Engineering, Monash University, Clayton VIC 3800, Australia

Abstract

This study investigates the effects of the application of various boundary conditions on the dynamics of flows within a rotating convection cell forced through a single differentially heated boundary. Several rotating horizontal convection flows were computed in a cylindrical enclosure, varying the boundary conditions applied on the base and lid of the container. Despite the flows still being in adjustment, significantly higher instantaneous Nusselt numbers are acquired when the thermally forced boundary is co-located with a stress-free boundary. The same cases also result in flows with higher kinetic energies and eddy activity. This possibly increases the rate of mixing in such a system. The fully confined non-slip container instead showed the lowest activity, and so caution must be exercised when extrapolating experimental data to oceanic scales when using such a setup.

Keywords

rotating flows; natural convection; ocean circulation.

Introduction

The global overturning circulation of the ocean is crucial in its role in the transport of scalars such as heat, salt and bionutrients, and acts to regulate the global climate [4, 29]. While wind stress on the ocean is widely accepted to be the primary driver of the circulation, the role of surface buoyancy forcing remains in contention. Works by [16] amongst others (see review by [9]) have shown that horizontal convection, a class of flows driven by the application of non-uniform buoyancy forcing through a single surface, captures the essential components of the circulation such as the formation of a strong thermal boundary layer akin to the thermocline, the intense sidewall plume representative of sinking regions and deepwater formation, and the weak return flow similar to the slow upwelling observed in the oceans. The debate revolves around the ability of flows in horizontal convection to become turbulent as this is crucial in mixing and transport processes of the oceans, often citing the ‘anti-turbulence theorem’ by [11]. Experiments by [27] and [28] have also argued that horizontal convection produces negligible levels of mixing compared to those observed in the oceans after extrapolating their data from laboratory to oceanic scales. Numerous studies have since argued otherwise that flows in horizontal convection can indeed be turbulent and produce significant levels of mixing in the oceans [5, 17, 21], but uptake on the concept is still generally slow.

Including rotation into this setup permits a baroclinic mechanism [1, 12], which contributes strongly to oceanic transport. There is, however, a large degree of variability in the setup of the experiments investigating the same problem. The setup employed in [24, 26] was a fully enclosed container with thermal forcing applied at the base, emulating an ‘upside down’ ocean following [12] and the non-rotating setup by [5]. [25] used an identical setup, but also reported that stress-free zonal sidewalls produce similar results to the non-slip. [18, 30] utilised a free-surface lid and is thermally forced at the base to emulate a laboratory-realizable setup. [19, 20] used ocean-relevant

boundaries by thermally forcing the stress-free upper surface.

Several recent papers on the non-rotating setup [13, 14, 15] found notable differences in the heat transport properties of the flow depending on the boundary conditions applied, although the bulk dynamics of the flow remained similar. Underlying symmetries in the non-rotating setup make them more forgiving to such boundary condition permutations, but such symmetries are broken with rotation. To the best of our knowledge, the effects of such variations in the setup have yet to be methodically examined for rotating horizontal convection, thus motivating this study.

Methodology

The basic setup used in this study revolves around a water filled cylindrical enclosure of height-to-radius aspect ratio $AR = H/R = 0.4$ that is rotated about its axis at an angular velocity of Ω . In all cases, the cylinder side-wall is non-slip and adiabatic. The cylinder lid and base are prescribed permutations of both non-slip and stress-free boundaries, and buoyancy is forced through either the lid or the base of the container with a linear radially increasing function of temperature, the opposite boundary remaining adiabatic. These cases are summarised in table 1. For brevity, the boundary where thermal forcing is applied is denoted as S .

Case	Boundary	Condition
1	base (S) lid	no-slip, thermally forced, no-slip, adiabatic,
2	base lid (S)	no-slip, adiabatic, no-slip, thermally forced,
3	base (S) lid	no-slip, thermally forced, stress-free, adiabatic,
4	base lid (S)	no-slip, adiabatic, stress-free, thermally forced,
5	base (S) lid	stress-free, thermally forced, stress-free, adiabatic.

Table 1. Summary of the boundary conditions considered.

This flow is computed in an inertial frame and imposes rotation through moving solid surfaces. The governing equations are non-dimensionalised using the container radius R for lengths, $1/\Omega$ for time, $R\Omega$ for velocities, $\rho R^2 \Omega^2$ for pressure, and the difference in the thermal forcing imposed ($\Delta T = T_{\text{hot}} - T_{\text{cold}}$) for temperatures. The non-dimensional governing equations for a Boussinesq fluid with a linear equation of state thus take the form:

$$\nabla \cdot \mathbf{u} = 0, \quad (1)$$

$$\frac{D\mathbf{u}}{Dt} = -\nabla p + \frac{2}{QRa^{2/5}} \nabla^2 \mathbf{u} + \frac{4Ra^{1/5}}{Q^2 Pr} T \mathbf{e}_z, \quad (2)$$

$$\frac{DT}{Dt} = \frac{2}{QRa^{2/5} Pr} \nabla^2 T, \quad (3)$$

where $\mathbf{u}(z, r, \theta)$ is the velocity in cylindrical coordinates, p is the

pressure modified to include the gravitational potential, T is the nondimensional temperature, the Rayleigh, Prandtl and Ekman numbers are $Ra = g\alpha\Delta TR^3/\nu\kappa$, $Pr = \nu/\kappa$, and $E = \nu/R^2\Omega$, respectively (α , ν , and κ being the thermal expansion coefficient, viscosity, and thermal diffusivity of the fluid, respectively), and rotation here has been parameterised through Q which relates the thickness of the thermal boundary layer δ_θ to that of the viscous Ekman layer δ_E as $Q = 2(\delta_\theta/\delta_E)^2 = 2/(ERa^{2/5})$, assuming that the thermal and viscous boundary layer thicknesses scale by $\delta_\theta \sim Ra^{-1/5}$ and $\delta_E \sim E^{1/2}$ [6, 16]. All cases reported here are for $Pr = 6.14$, $Ra = 1 \times 10^9$ and $Q = 10$ ($E \approx 5 \times 10^{-5}$), the latter being chosen such that the flows lie within the ‘moderate’ to ‘strong rotation’ regime described by [8], and where [18] have shown that their linear instability mode possesses a baroclinic origin.

These equations are discretised using a nodal spectral-element method in the meridional semi-plane coupled with a Fourier expansion in the azimuth [3], and are evolved forward in time using a third-order multi-step scheme based on backwards differentiation [10]. The Fourier basis functions used in the discretisation of variables in the azimuth naturally impose a periodic boundary, thus completing the cylinder. An in-house solver is used, which has been implemented and validated across various problems, some of which can be found in [18, 22, 23]. Overall, the meridional semi-plane possesses 1274 spectral elements each utilising an 8th-order Lagrangian polynomial interpolant, and either 96 or 192 azimuthal Fourier modes. The initial states used for these computations were their respective axisymmetric solutions which have been evolved to an asymptotic envelope, and were perturbed by white noise to facilitate instability.

Some preliminary results

The remainder of this paper will present some preliminary results to demonstrate the extent to which the different surface boundary conditions affect the asymptotic states of the flow. We emphasize first that some of the results presented are still in transient adjustment and have yet to equilibrate, but are well past the point where strong nonlinearities have set in (figure 1). Specifically, case 1 is statistically stationary while cases 2–5 are not. The long adjustment times of the flows in horizontal convection are well known [7], some of the present cases having been in computation for several months.

As a starting point, the differences between the thermal fields of the various boundary condition combinations on the axisymmetric flow are first elucidated in figure 2. These axisymmetric solutions with an azimuthally uniform velocity field are noticeably different, particularly in regions where the thermal plume driving the overturning circulation forms. Case 1 is the only case that was observed to develop a strong thermal boundary layer reminiscent of the ocean’s thermocline, while case 2 shows a similar but weaker thermal layer. These result in larger thermal fluxes through the forcing boundary S , which explains the larger values at initialisation in figure 1. The remaining cases show an outcropping of the isotherms through the boundary opposite to S , and along with consideration of their available potential energies, indicate that they can be baroclinically unstable. As shown in [1] and [18], one can increase the likelihood of inciting baroclinic instability by increasing the system’s rotation. The thermal fields of case 1 and case 3 in figure 2 in particular resemble those for $Q = 1$ and $Q = 10$ from figure 2 of [18] (identical setup to case 3 here), leading one to anticipate that case 1 with the solid surface boundaries might require at least a 10-fold or order-of-magnitude increase in the rotation rate to achieve a similar susceptibility to baroclinicity.

For the three-dimensional flows, the initially perturbed two-

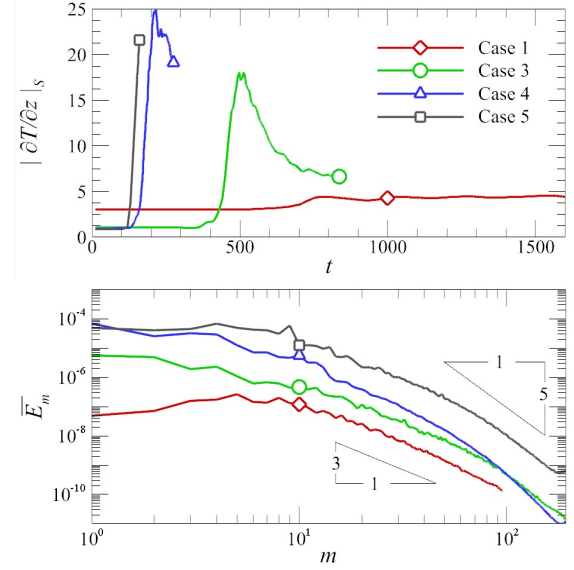


Figure 1. (Top) Transient adjustment of the surface boundary flux along S , and (bottom) the time-averaged Fourier energy spectra, where m is the azimuthal wavenumber.

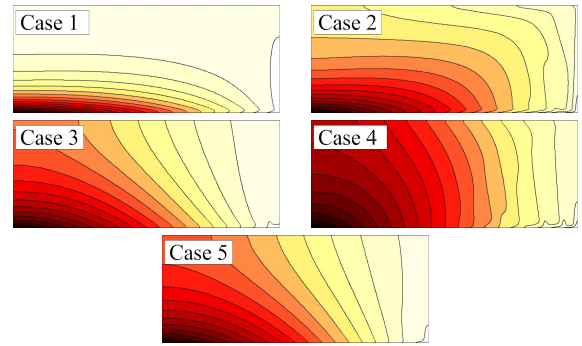


Figure 2. Temperature fields in the meridional semi-plane of the axisymmetric flow for the cases as labelled inset. The axes and colourmap of cases 2,4 have been inverted for coherence with the remaining plots.

dimensional axisymmetric flows rapidly become unstable. Cases 4 and 5, where the forcing boundary S is accompanied by a free surface, show that linear growth is arrested in less than half the time taken by cases 1 and 3 where S is applied on a solid surface, indicating that instabilities grow more aggressively when the forcing boundary is free-slip, regardless of whether it is applied on the top or bottom of the domain. Case 2 has yet to evolve for a sufficient period of time, and so they are not considered in this discussion.

Figure 1 shows how the surface thermal flux on S evolves over time. The latency in the breakdown of linear growth for cases 1 and 3 described above can also be observed here. Most importantly, this figure demonstrates that surface fluxes on the forcing boundary S are immensely stronger during the transient adjustment stage when they are applied on a stress-free boundary (cases 4 and 5). The surface flux when the forcing boundary is prescribed on a solid surface but with a stress-free boundary on the opposing side (case 3) is also still much larger than that where the confines are fully solid (case 1). Note here again, however, that cases 3–5 have yet to equilibrate. The accompanying plot of the mean Fourier energies within the flow shows that most of the energy resides at lower wavenumbers in all cases, and that $E_m \sim m^{-3}$ after the spectral rolloff, increasing

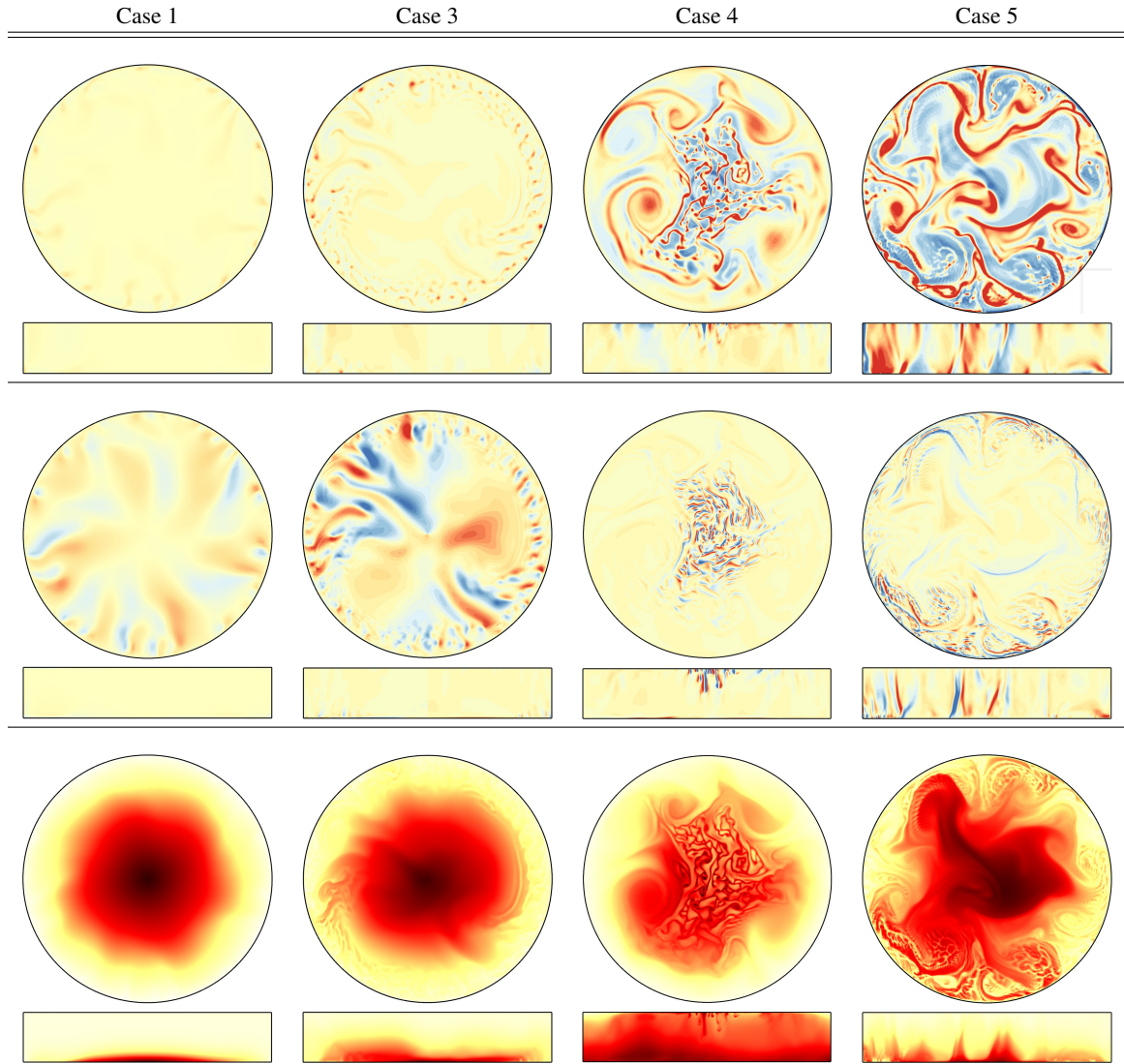


Figure 3. Surface and center cross-section plots of the eddy z -vorticity (ζ'_z), θ -vorticity (ζ_θ), and temperature fields (T) from top to bottom, shown for cases labelled in the column heading. The surface sections shown are at an axial distance of $0.0125H$ from S , and contour levels have been set over ranges $\zeta'_z = \zeta_\theta \in [-2, 2]$ and $T \in [0, 1]$.

further at higher wavenumbers. This serves to validate our results with the similar spectral slope reported by [2]. It can also be observed here that the magnitudes of the Fourier energies are much higher in cases 4 and 5 (forcing boundary on a free-surface) than in cases 1 and 3 (forcing boundary on a no-slip solid surface), indicating much higher levels of eddy activity (kinetic energy). This is elucidated through a series of flow visualisations presented in figure 3. The eddies of lengths of $O(R)$ in the surface z -vorticity for cases 4 and 5 along with the smaller eddies that are shed from them in case 4 are known to be important in the transport of scalars in the oceans [29]. In case 4, the intense small-scale eddying features are shed from the fronts of the larger eddies, and are biased towards the convergence zone resulting in downwelling plumes, while in case 5 these eddies develop at the periphery. While not explicitly calculated, one speculates that the stronger eddying motions and convection observed in the free-surface cases will lead to stronger mixing rates, thus affecting the overall mixing efficiency of the system.

Conclusions

The choice of boundary conditions should always reflect the

physical setup being modelled, but in complex systems such as the oceans, it is common to use idealised models or geometries on which one can investigate its physics with academic rigour. In such setups, combinations of both non-slip and stress-free boundaries on the base and lid of the convection cell can almost always be justified. The results in this paper, however, demonstrates how free-surfaces or stress-free boundaries in the convection cell increases the strength of convection and eddy activity compared to the corresponding setup with no-slip boundaries. The results herein thus call for various studies to exercise some degree of caution in extrapolating numerical or experimental results to geophysically relevant scales depending on the boundary conditions used in their setup.

Because of the focus on boundary condition effects in this study, there are several limiting aspects of this investigation, especially considering the geophysical motivation. The flows in this study are in an f -plane with a constant Coriolis acceleration, neglecting the more complex β -plane effects associated with latitude-dependence of Coriolis effects. Another crucial ingredient omitted here is the inclusion of wind stresses which can drive the circulation. Other factors such as the consideration of

stratification through salinity gradients, and the possibility of a nonlinear equation of state were also excluded. This study has also chosen to focus on a single Rayleigh number and rotation rate to permit direct comparisons, and so the effects of Ra and Q variations have yet to be explored in this context. It is unclear whether these will significantly alter the results, and would form the basis of further investigations in the future.

Acknowledgements

This research was supported by the Australian Research Council through Discovery Grant DP180102647, and was undertaken with the assistance of resources provided by the Monash eResearch Centre through the use of the MonARCH HPC Cluster, Pawsey Supercomputing Centre with funding from the Australian Government and the Government of Western Australia, and the National Computational Infrastructure (NCI) which is supported by the Australian Government.

References

- [1] Barkan, R., Winters, K. B. and Llewellyn Smith, S. G. (2013). Rotating horizontal convection, *J. Fluid Mech.*, 723, 556–586.
- [2] Barkan, R., Winters, K. B. and Llewellyn Smith, S. G. (2015). Energy cascades and loss of balance in a reentrant channel forced by wind stress and buoyancy fluxes, *J. Phys. Oceanogr.*, 45, 272–293.
- [3] Blackburn, H. M. and Sherwin, S. J. (2004). Formulation of a Galerkin spectral element-Fourier method for three-dimensional incompressible flows in cylindrical geometries, *J. Comput. Phys.*, 197, 759–778.
- [4] Cessi, P. (2019). The global overturning circulation, *Annu. Rev. Mar. Sci.*, 11, 249–270.
- [5] Gayen, B., Griffiths, R. W. and Hughes, G. O. (2014). Stability transitions and turbulence in horizontal convection, *J. Fluid Mech.*, 751, 689–724.
- [6] Greenspan, H. P. (1968). *The theory of rotating fluids*, Cambridge Monographs on Mechanics and Applied Mathematics, Cambridge University Press.
- [7] Griffiths, R. W., Hughes, G. O. and Gayen, B. (2013). Horizontal convection dynamics: insights from transient adjustment, *J. Fluid Mech.*, 726, 559–595.
- [8] Hignett, P., Ibbetson, A. and Killworth, P. D. (1981). On rotating thermal convection driven by non-uniform heating from below, *J. Fluid Mech.*, 109, 161–187.
- [9] Hughes, G. O. and Griffiths, R. W. (2008). Horizontal convection, *Annu. Rev. Fluid Mech.*, 40, 185–208.
- [10] Karniadakis, G. E. and Triantafyllou, G. S. (1992). Three-dimensional dynamics and transition to turbulence in the wake of bluff objects, *J. Fluid Mech.*, 238, 1–30.
- [11] Paparella, F. and Young, W. R. (2002). Horizontal convection is non-turbulent, *J. Fluid Mech.*, 466, 205–214.
- [12] Park, Y.-G. and Whitehead, J. A. (1998). Rotating convection driven by differential bottom heating, *J. Phys. Oceanogr.*, 29, 1208–1220.
- [13] Passaglia, P.-Y., Scotti, A. and White, B. (2017). Transition and turbulence in horizontal convection: linear stability analysis, *J. Fluid Mech.*, 821, 31–58.
- [14] Reiter, P. and Shishkina, O. (2020). Classical and symmetrical horizontal convection: detaching plumes and oscillations, *J. Fluid Mech.*, 892, R1.
- [15] Rocha, C. B., Constantinou, N., Llewellyn Smith, S. G. and Young, W. R. (2020). The Nusselt numbers of horizontal convection, *J. Fluid Mech.*, 894, A24.
- [16] Rossby, H. T. (1965). On thermal convection driven by non-uniform heating from below: an experimental study, *Deep-Sea Res.*, 12, 9–16.
- [17] Scotti, A. and White, B. (2011). Is horizontal convection really “non-turbulent?”, *Geophys. Res. Lett.*, 38, L21609.
- [18] Sheard, G. J., Hussam, W. K. and Tsai, T. (2016). Linear stability and energetics of rotating radial horizontal convection, *J. Fluid Mech.*, 795, 1–35.
- [19] Sohail, T., Gayen, B. and Hogg, A. M. (2018). Convection enhances mixing in the Southern Ocean, *Geophys. Res. Lett.*, 45, 4198–4207.
- [20] Sohail, T., Vreugdenhil, C. A., Gayen, B. and Hogg, A. M. (2019). The impact of turbulence and convection on transport in the Southern Ocean, *J. Geophys. Res. Oceans*, 124, 4208–4221.
- [21] Tailleux, R. (2009). On the energetics of stratified turbulent mixing, irreversible thermodynamics, Boussinesq models and the ocean heat engine controversy, *J. Fluid Mech.*, 638, 339–382.
- [22] Tsai, T., Hussam, W. K., King, M. P. and Sheard, G. J. (2020). Transitions and scaling in horizontal convection driven by different temperature profiles, *Int. J. Thermal Sci.*, 148, 106166.
- [23] Vo, T., Montabone, L., Read, P. L. and Sheard, G. J. (2015). Non-axisymmetric flows in a differential-disk rotating system, *J. Fluid Mech.*, 775, 349–386.
- [24] Vreugdenhil, C. A., Gayen, B. and Griffiths, R. W. (2016). Mixing and dissipation in a geostrophic buoyancy-driven circulation, *J. Geophys. Res. Oceans*, 121, 6076–6091.
- [25] Vreugdenhil, C. A., Gayen, B. and Griffiths, R. W. (2019). Transport by deep convection in basin-scale geostrophic circulation: turbulence-resolving simulations, *J. Fluid Mech.*, 865, 681–719.
- [26] Vreugdenhil, C. A., Griffiths, R. W. and Gayen, B. (2017). Geostrophic and chimney regimes in rotating horizontal convection with imposed heat flux, *J. Fluid Mech.*, 823, 57–99.
- [27] Wang, F., Huang, S.-D. and Xia, K.-Q. (2018). Contribution of surface thermal forcing to mixing in the ocean, *J. Geophys. Res. Oceans*, 123, 855–863.
- [28] Wang, W. and Huang, R. X. (2005). An experimental study on thermal circulation driven by horizontal differential heating, *J. Fluid Mech.*, 540, 49–73.
- [29] Wunsch, C. and Ferrari, R. (2004). Vertical mixing, energy, and the general circulation of the oceans, *Annu. Rev. Fluid Mech.*, 36, 281–314.
- [30] Zhang, Y., Chen, C., Zhang, Z. and Wang, W. (2016). Rotating horizontal convection and the potential vorticity constraint, *J. Fluid Mech.*, 803, 72–93.